Nuclear Instruments and Methods in Physics Research A 613 (2010) 263–271

Contents lists available at ScienceDirect

Nuclear Instruments and Methods in Physics Research A

journal homepage: www.elsevier.com/locate/nima

Geant4 simulation of the solar neutron telescope at Sierra Negra, Mexico

L.X. González [a,*], F. Sánchez [b], J.F. Valdés-Galicia [a]

[a] Instituto de Geofísica, Universidad Nacional Autónoma de México, 04510 D.F. México, México
[b] Comisión Nacional de Energía Atómica, 1429 Buenos Aires, Argentina

ARTICLE INFO

Article history:
Received 20 October 2009
Accepted 26 November 2009
Available online 3 December 2009

Keywords:
Detector simulation
Geant4
Solar neutrons

ABSTRACT

The solar neutron telescope (SNT) at Sierra Negra (19.0°N, 97.3°W and 4580 m.a.s.l) is part of a worldwide network of similar detectors (Valdés-Galicia et al., (2004) [1]). This SNT has an area of 4 m^2; it is composed by four 1 m × 1 m × 30 cm plastic scintillators (Sci). The Telescope is completely surrounded by anti-coincidence proportional counters (PRCs) to separate charged particles from the neutron flux. In order to discard photon background it is shielded on its sides by 10 mm thick iron plates and on its top by 5 mm lead plates. It is capable of registering four different channels corresponding to four energy deposition thresholds: $E > 30$, > 60, > 90 and > 120 MeV. The arrival direction of neutrons is determined by gondolas of PRCs in electronic coincidence, four layers of these gondolas orthogonally located underneath the SNT, two in the NS direction and two in the EW direction. We present here simulations of the detector response to neutrons, protons, electrons and gammas in range of energies from 100 to 1000 MeV. We report on the detector efficiency and on its angular resolution for particles impinging the device with different zenith angles. The simulation code was written using the Geant4 package (Agostinelli et al., (2003) [2]), taking into account all relevant physical processes.

1. Introduction

Solar neutrons are produced by nuclear reactions of solar flare-accelerated protons and nuclei [3]. The production of neutrons is accompanied by gamma-ray emission, since the first neutrons produced are emitted toward the solar interior, these may be captured by photospheric hydrogen and release of a characteristic γ-ray line at 2.223 MeV. Furthermore, detected γ-ray lines at 0.511, 4.4 and 6.1 MeV are produced by annihilation of energetic positrons from the decay of positive pions, nuclear deexcitation of carbon and oxygen, respectively. The neutral pions decay directly into two 67.5 MeV γ-rays.

Magnetic reconnection is a likely process for particle acceleration at solar flares. The magnetic free energy is stored in the corona, due to either motion of the photospheric footpoints of loops or the emergence of current-carrying field from below the photosphere.

The collision of magnetic loops might lead to reconnection that will in turn heat up the solar plasma. This hot plasma blows downward and hits the top of magnetic loop, where the particles are accelerated by collision with this plasma jet [4]. The accelerated particles follow the field lines and interact with the chromospheric gas where they may generate nuclear reactions (p^+–p^+, p^+–α, α–α) that produce neutrons.

The detection of solar neutrons is very important since they are not affected by magnetic fields; therefore, they preserve information to understand the acceleration mechanism of ions at the solar atmosphere; i.e. the starting time of ion acceleration and to determine if the process is gradual or instantaneous.

The first measurement of solar neutrons was done by the *Solar Maximum Mission* Satellite from the solar flare of June 21, 1980 as is described in [5]. For the solar flare of June 3, 1982 high energy solar neutrons were first detected at earth by ground level neutron monitors [6].

On the ground, we can measure solar neutrons with kinetic energy greater than 100 MeV, because they are strongly attenuated in the Earth's atmosphere.

On June 4, 1991 the SNT at Mt. Norikura was the first solar neutron telescope to measure solar neutrons. Muraki et al. [7] assumed an impulsive injection at the solar atmosphere, and calculated a spectral power index ($\gamma = -5.4$).

For the solar cycle 23, some solar neutron events were detected by SNTs as shown in [4]. They conclude that the observation of solar neutron events is an important tool to understand solar particle acceleration mechanism and SNTs have proved to be useful to study solar neutrons.

For the X17 solar flare of September 7, 2005 the SNT at Sierra Negra, detected a very strong solar neutron emission. GOES satellite observed a soft X-ray maximum at 17:40 UT. In [8] it was

* Corresponding author. Tel.: +52 55 5616 1480; fax: +52 55 5550 2486.
E-mail address: xavier@geofisica.unam.mx (L.X. González).

0168-9002/$ - see front matter © 2009 Elsevier B.V. All rights reserved.
doi:10.1016/j.nima.2009.11.074

shown that a δ-function injection and a simple power law spectrum are not sufficient to explain the neutron extended emission signal detected. Using the carbon nuclear de-excitation line emission and a spectral power index ($\gamma = -3.1$), Watanabe et al. [9] obtained a close fit to the neutron data time profile. For this solar neutron event, the spectral power index seems to be about -3, according with [10], where they used Monte Carlo simulations of the SNT response.

2. The solar neutron telescope

From June 2004, the SNT at Sierra Negra has been taking data and it is ready for the solar cycle 24. This detector is the newest of the solar neutron telescope network (Fig. 1). A schematic view of the SNT at Sierra Negra is shown in Fig. 2.

The SNT consists of four 30 cm thick plastic scintillators (Sci) surrounded by gondolas of proportional counters (PRC) to detect charged particles. These PRCs are in electronic anti-coincidence with the Sci that can register charged and neutral particles. Incident particles collide with carbon nucleus of the Sci and release protons (p^+), by the reaction $n+{}^{12}C \rightarrow p^+ + X$. These recoil p^+ may be detected by four orthogonal PRCs underneath the SNT (two are in the N–S direction, and other two in the E–W); therefore we can determine the arrival direction of the incident particles, classifying in five regions for each orthogonal PRC. This design is enough to estimate the original incoming neutron direction with an accuracy of 15°, as counting rates are measured for each of the 25 possible hit patterns in the two possible directions (N–S and E–W, see Fig. 10).

Based on the electronic anti-coincidence we can discriminate between charged and neutral particles (Fig. 2).

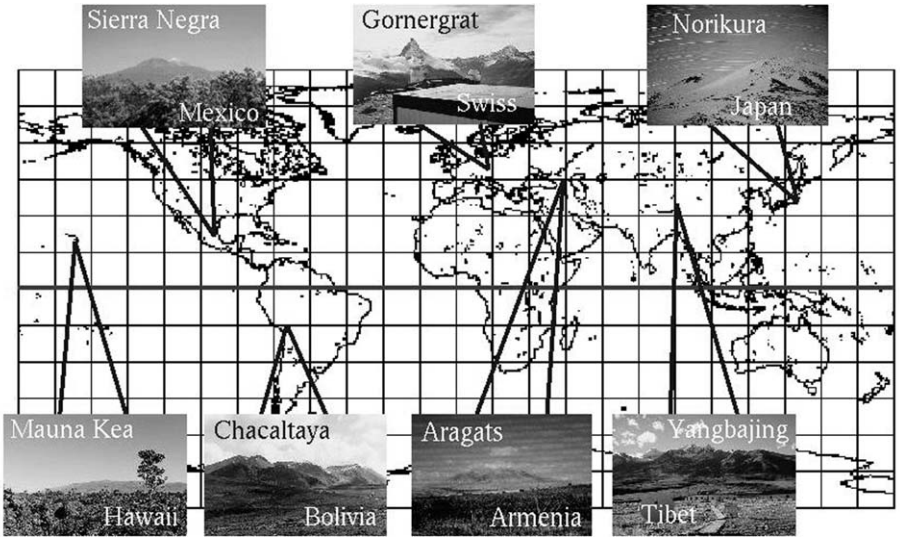

Fig. 1. The worldwide solar neutron telescope network (http://stelab.nagoya-u.ac.jp/ste-www1/div3/CR/neutron/index.html).

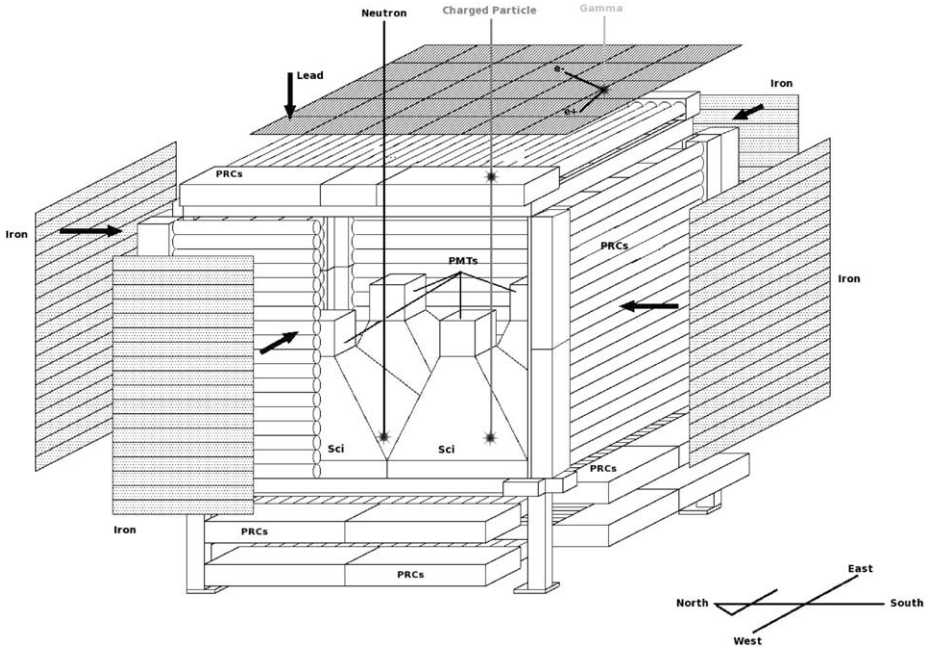

Fig. 2. Schematic view of the SNT at Sierra Negra, showing the electronic anti-coincidence signal between charged and neutral particles and all other active components of the detector (see Section 2).

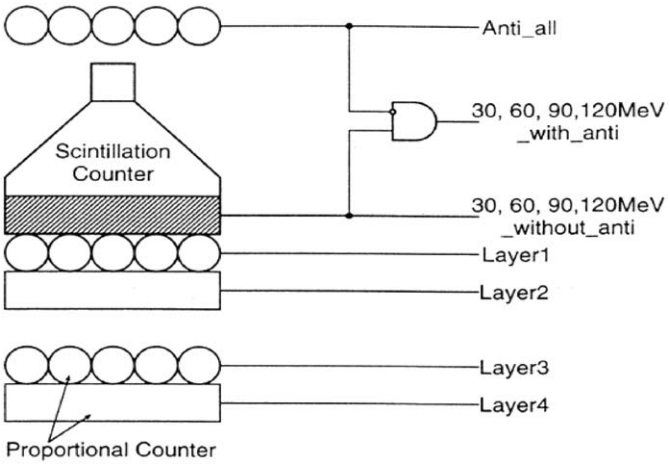

Fig. 3. Electronic discriminator for different channels of SNT, showing the anti-coincidence for four energy deposition thresholds (> 30, 60, 90 and 120 MeV). Neutrons have the subscript *_with_anti*, and charged particles the subscript *_without_anti*. The four layers underneath the scintillator are the orthogonal PRCs to detect the recoil P^{+}.

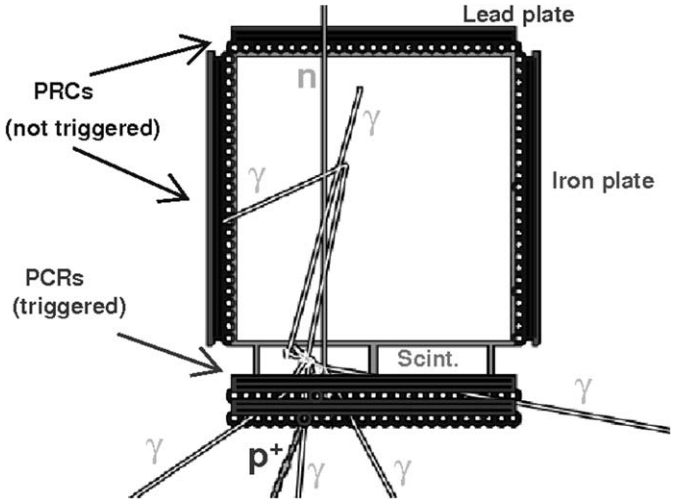

Fig. 4. An example of the simulation output. One impinging vertical neutron (n) interacts in the plastic scintillator and produces a recoil proton (p^{+}) that triggers four PRCs underneath the Sci. The anti-coincidence with respect to the top PRCs is the typical signature of a neutral particle crossing the telescope sensitive volume. This figure shows an example of an internal production of low energy gammas by nuclear reaction inside the Sci, four gammas leave the detector, another is absorbed in the air and the last one is absorbed by the iron plate.

The energy deposited (E_{dep}) by neutrons is measured by pulse height discriminators connected to the photomultiplier (PMT) installed above each Sci in a light tight pyramid (see Figs. 2 and 3). The pulse height is discriminated and registered in four different energy deposition thresholds channels (Fig. 3) that correspond to $E > 30$ MeV (*S1_with_anti*), $E > 60$ MeV (*S2_with_anti*), $E > 90$ MeV (*S3_with_anti*) and $E > 120$ MeV (*S4_with_anti*).

To reduce the contamination by other particle species, the TNS is shielded on top by a layer of lead (5 mm thick) and on the four vertical sides by iron plates (10 mm thick). In this way, the signals of γ- and α-particles, that could contaminate the neutron signal, are minimized.

In this paper we will present the full simulation of SNT at Sierra Negra, taking into account all the active components of the detector and relevant physical process, for n, γ, p^{+} and e^{-} entering the telescope with three different zenith angles and a range of energies from 100 to 1000 MeV.

3. Simulation description

It is relevant to know whether the detection capability of our telescope is adequate and is not contaminated by other particle species. It is very important to take accurate measurements of solar neutrons, in order to determine the solar neutron flux at the Earth and reconstruct the corresponding flux at the solar atmosphere, in order to estimate the most appropriate spectrum of accelerated ions at solar flares.

Simulations to know the response of the SNT installed at Mt. Aragats [11] and at Gornergrat [12] were done using the GEANT3 code. A partial simulation of our detector to know the response of the plastic scintillators was performed previously [1]. In this work we have simulated all the detector active components: the proportional counters, the iron and lead plates, and the plastic scintillators. In each of these materials, the simulation package takes into account all the physical processes relevant to *particles passing through matter*. These processes are density effects, electromagnetic processes (*gammas*: photo-electric effect, Compton scattering; *electron:* ionization, energy losses, Bremsstrahlung, e^{+}–e^{-} annihilation; *charged hadrons*: ionization, energy loss; *charged particles*: multiple scattering, transition radiation, scintillation, Cherenkov radiation) and nuclear interactions (n–p^{+}, p^{+}–p^{+}, ^{12}C–p^{+}, ^{12}C–n) [2]. Default and different cross-section sets are provided automatically for each type of hadronic process, particles and materials.

As an example, we show in Fig. 4 the graphical output of the simulation of a vertical impinging neutron of 0.5 GeV. As can be seen, the rationale behind the detection technique is very simple: all neutral particle detectors require that the neutral particle have an interaction that results in the liberation of a charged particle somewhere within its sensitive volume; in our case, neutrons (n) have a very small probability of interacting with the top lead plates and eventually trigger the proportional counters on the top of the telescope; nevertheless, because the plastic scintillators are hydrogen-rich compounds, they have a relative high chance of producing a recoil proton (p^{+}) or another charged secondary while crossing the plastic (by means of either elastic scattering or inelastic reactions); in this way, a neutron can be distinguished from charged particles (such as protons) because its pattern in the detector will be an anti-coincidence signal between the top or sideways PRCs accompanied by a signal arising from the deposition of energy in the scintillators.

Nevertheless there are some issues that push against the above simple argument and compete with the detection efficiency of the SNT. First of all, some neutrons may go through the whole telescope without interacting or, on the contrary, interact within the lead plate or the gas of the PRC above the Sci. Another possibility is that the recoil products of the reaction inside the scintillators will not reach the PRC beneath the scintillators or, if they are sufficiently energetic to be pulled out of the plastics, they might not trigger the four PRCs, necessary condition to have an angular reconstruction of the event [13].

There are some other events that may be mistakenly assigned as neutron events. That is the case of high energy photons. In fact, photons can go through the top PRCs and convert to an electron–positron pair in the scintillators leaving a *neutron-like* signature. To reduce this effect, the SNT has on its roof a lead plate of 5 mm thickness. In this way, most of the gammas will convert in the top of the telescope producing a coincident signal (e^{+}–e^{-} pair). High energy protons would also have a chance of producing a *neutron-like* signature, i.e. they are not detected by the PRCs and are detected by Sci (*anti-coincidence signal*). These signals would

contaminate our neutron counts. The only possibility to have an estimate of their importance is through a detailed numerical simulation.

4. Simulation results

We have simulated 5×10^4 incident particles of each of the relevant species: neutrons, gammas, protons and electrons hitting the detector with energies in the range 100 MeV to 1 GeV using Geant4 [2] as the core of our numerical code. We studied the case of 3 different impinging zenith angles: 0°, 30° and 60°. We consider only anti-coincidence type of events that additionally trigger the four proportional counters of the bottom layers in order to also have an angular reconstruction of the event.

The electronic signal in the PMTs is proportional to the energy released by neutral and charged particles in the scintillators (E^{sci}_{dep}). In this way, we emulate the response of each telescope channel.

The different detector channels may be used to estimate the modifications of the spectrum of the incident neutrons as can be seen in Fig. 5. This figure shows the relationship between the primary energy (E_{inj}) of neutrons and the energy deposited in the Sci by these neutrons, for the three different zenith angles considered. We can see that incident neutrons (for 0°, 30° and 60° incident angles) with 100 MeV of primary energy (E_{inj}) deposit more than 30 MeV on the Sci; in this way, all of them are detected by the channel *S1_with_anti* ($E_{dep} \geq 30$ MeV). Neutrons with E_{inj} greater than 600 MeV always deposit at least 120 MeV and will be detected by the four neutron channels.

Neutrons with impinging zenith angles of 0° and 30° are very similar from 300 MeV to 1 GeV of primary energy, unlike neutrons with 60° of impinging zenith angle; the difference is because, at 60° the neutrons traverse more of the Sci material and they deposit more energy. For all zenith angles, the neutrons that deposit 60 MeV in the Sci (E^{dep}_{sci}) have ~160 MeV of E_{inj}, but for neutrons with E^{dep}_{sci} greater than 60 MeV, the E_{inj} is a function of the zenith angle. For example, neutrons with 500 MeV of E_{inj} deposited 105, 110 and 140 MeV for 0°, 30° and 60° of zenith angle, respectively.

4.1. Particle detection efficiency

An earlier simulation of the solar neutron telescope [1] demonstrated that for the very energetic solar neutrons ($E \geq 500$ MeV), the detection efficiency would always be greater than 10%. Nevertheless, that estimate was limited to the plastic scintillators and did not take into account the proportional counter gondolas, the lead and iron plates. Every neutron producing a recoil proton in the scintillator was considered to be detected. This is not always the case in a more realistic situation. It is possible that the proton is not pulled out from the scintillator or, if so, does not trigger the four PRCs of the bottom gondolas. If these effects are taken into account, the efficiency is reduced. In this work, we have included all the above mentioned possibilities, and the results are shown in Fig. 6. It can be seen that the most sensible channel, *S1_with_anti*, has ~8–10% while *S4_with_anti*~ has 3–6% efficiency for $E_{inj} \geq 500$ MeV at all incident angles. In all cases, as expected, the efficiency increases with increasing zenith angle.

The neutrons have a larger path inside the scintillator as the incident angle is greater, and they are more likely to be detected. In this way, for neutrons with *inj* energy of 500 MeV and 0°, 30° and 60° of zenith angle, the maximum detection efficiency is 9.1%, 9.5% and 12.5%, respectively.

The probability that high energy protons produce a *contamination-signature* (*neutron-like* signal) is negligible; they are rejected by its coincidence signal in more than 99%. Fig. 7 shows the proton detection efficiency in terms of proton *inj* energy. The variations are negligible because, for protons with *inj* energy of 600 MeV and 0°, 30° and 60° of zenith angle, the detection efficiency is 0.012%, 0.62% and 0.41%, respectively.

For electrons, the simulation shows that the maximum contamination (*neutron-like* signal) is less than 2.5% (Fig. 8). For example, for electrons with 0°, 30° and 60° zenith angles, the *anti-coincidence* signals are 1.06%, 2.4% and 1.25%, respectively. But,

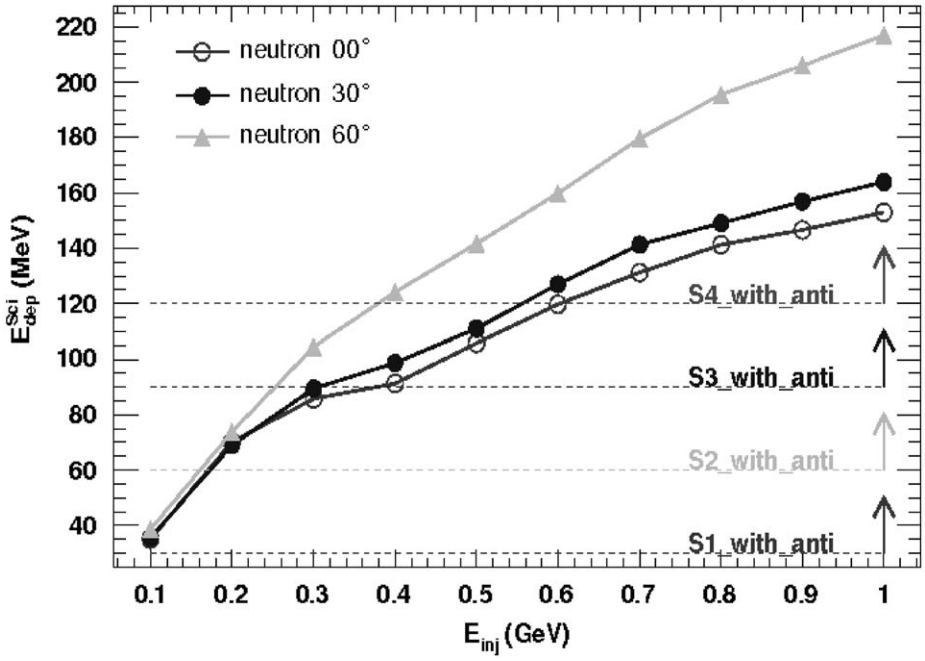

Fig. 5. Energy deposited by the impinging neutrons in the scintillators, E^{dep}_{sci}, as a function of their incident energies, E_{inj}. The different channels threshold allows an estimate of the neutron spectrum.

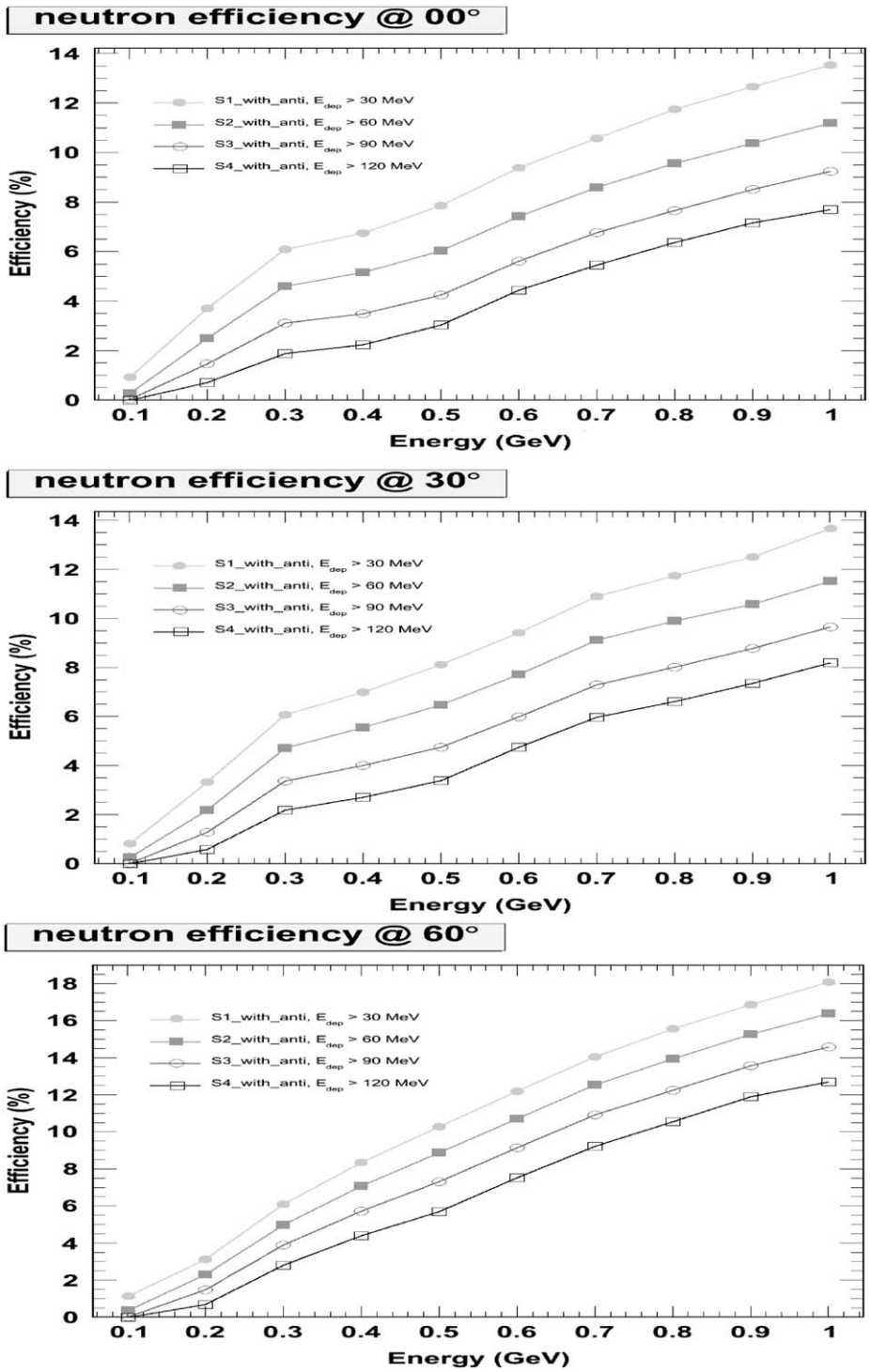

Fig. 6. Detection efficiencies of neutrons for incident zenith angle at 0° (top), 30° (middle) and 60° (bottom). The curves in each panel correspond to one out of the four acquisition channels.

the real flux of electrons at the level of our SNT is less than $1\ m^{-2}\ s^{-1}\ sr^{-1}$[14].

Finally, in the case of incident gammas, the simulation shows that adding the converted photon in the top lead plates, which produce a coincidence signal (*proton-like* signal) with those photons that are transparent to the detector, more than 65% of the photon background is rejected. This result, in complete agreement with [1], is almost independent of the incident energy or angle. In Fig. 9 we can see the contamination of high energy gammas.

As expected, the *contamination-signal* increases with zenith angle, i.e., for gammas with *inj* energies of 300 MeV, the maximum *contamination detection* is 5%, 5.5% and 9% for 0°, 30° and 60°, respectively.

Assuming a flux of gammas that is comparable with that of the neutrons, the *contamination-signal* of gammas with *inj* energies of 100 MeV is ~3.5% for all zenith angles, as shown in Fig. 9; this will hardly be the case in a realistic situation. It is very important to stress that the real flux of gammas with energies greater than 100 MeV at the level of our SNT is negligible ($\sim 1\ m^{-2}\ s^{-1}\ sr^{-1}$), [15,[16]].

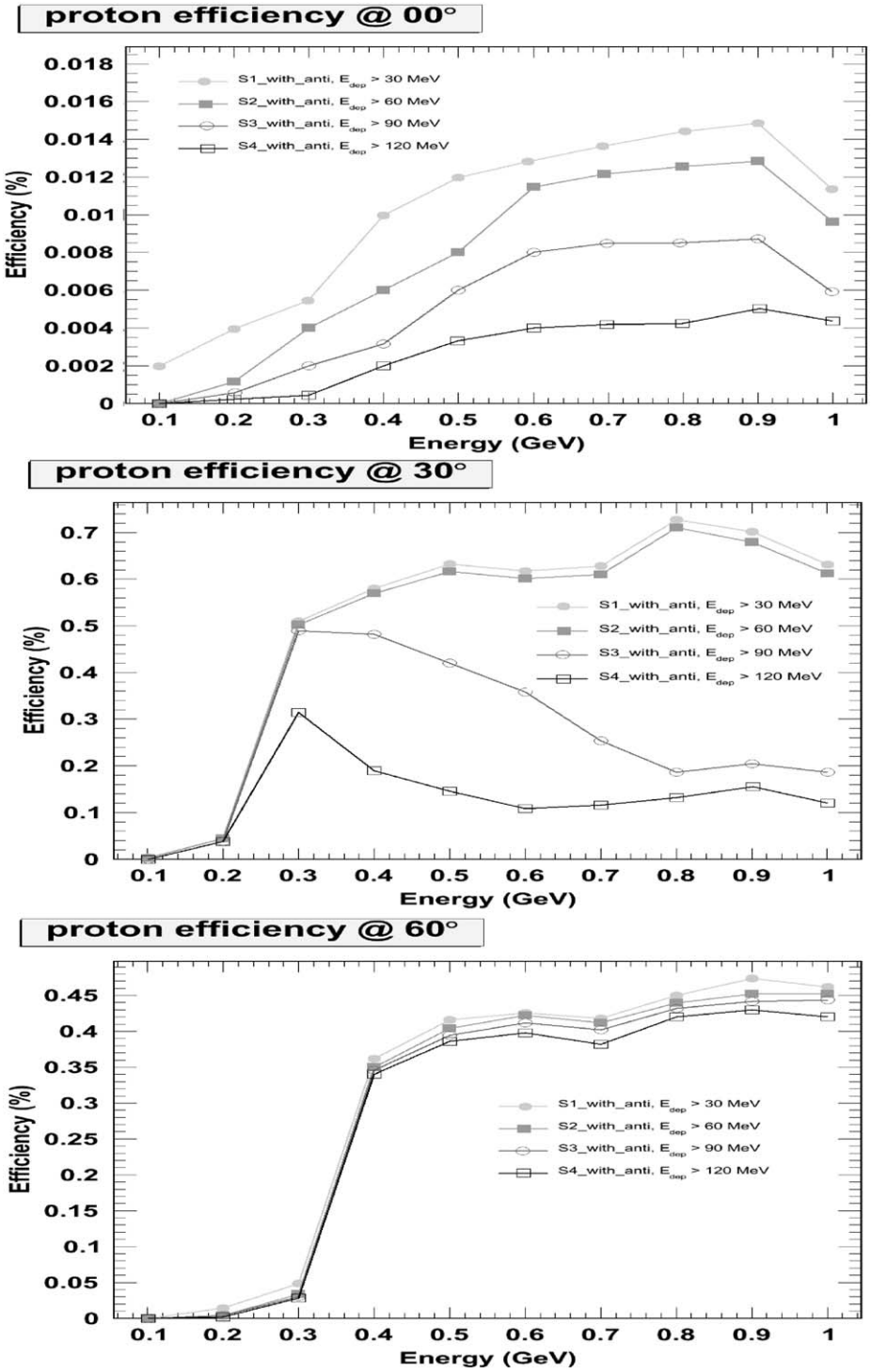

Fig. 7. Detection efficiencies of protons for incident zenith angle at 0° (top), 30° (middle) and 60° (bottom). Protons are rejected by more than 99%.

4.2. Angular resolution

The angular reconstruction of the telescope is provided by the simulation of the proportional counters located underneath the scintillators. As explained in Section 2, these 2 layers of PRCs allow classifying the direction of the recoiling proton (which is, in turn, correlated to the incoming neutron direction) in a 5×5 angular matrix of 15° resolution. The field of view is ~60° in the North–South and East–West directions.

The SNT carries out this process on line by means of specific logic circuits. The simulation code we produced is capable of estimating how the reconstructed angular directions are correlated with the true incoming direction, because it takes into account the simulation of all the PRCs.

As an example, Fig. 10(a) shows the case of a simulated solar neutron flux arriving vertically to the telescope (*mid-day* incoming flux). In this case, we have considered a flux of neutrons with energies from 100 MeV to 1 GeV.

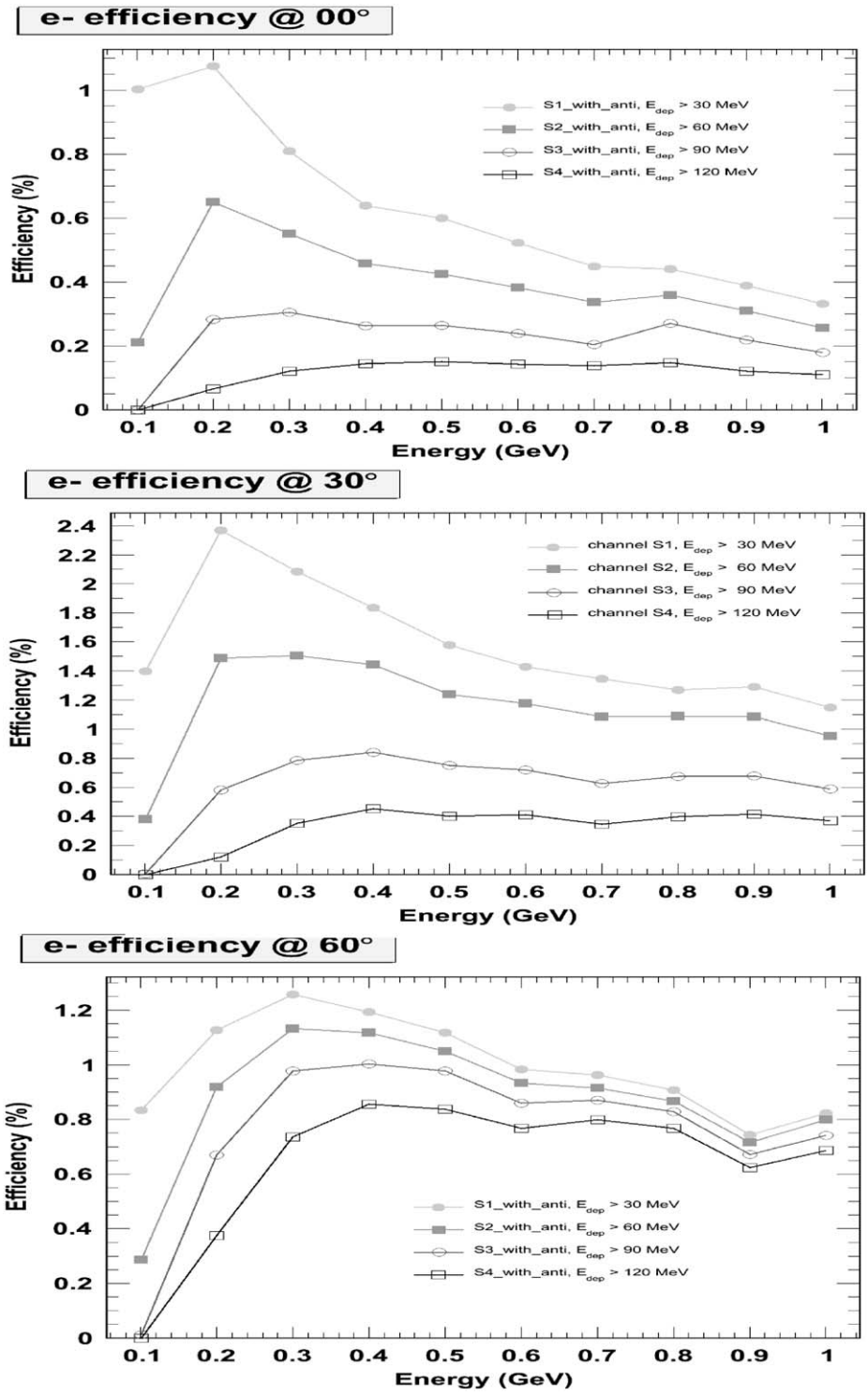

Fig. 8. Detection efficiencies of electrons for incident zenith angle at 0° (top), 30° (middle) and 60° (bottom), assuming a flux of electrons comparable to flux of neutrons. Electrons are rejected by more than 97%.

Around 11% of the reconstructed angles fall in the central pixel, while in its first neighboring pixels there are less than 6% of the events. Fig. 10(b) shows the real proportion of SNT counting rates during the event on September 7, 2005 at 11:40 LT. As can be appreciated there is a very good agreement between real and simulated data, giving us confidence that we are reproducing quite reasonably the response of the solar neutron telescope.

5. Conclusions

We have constructed a numerical simulation program to study the response of the solar neutron telescope located at the top of the Sierra Negra volcano in eastern Mexico. The core of the code uses the Geant4 package, taking into account all the sensitive components of the detector and all the relevant nuclear and electromagnetic processes.

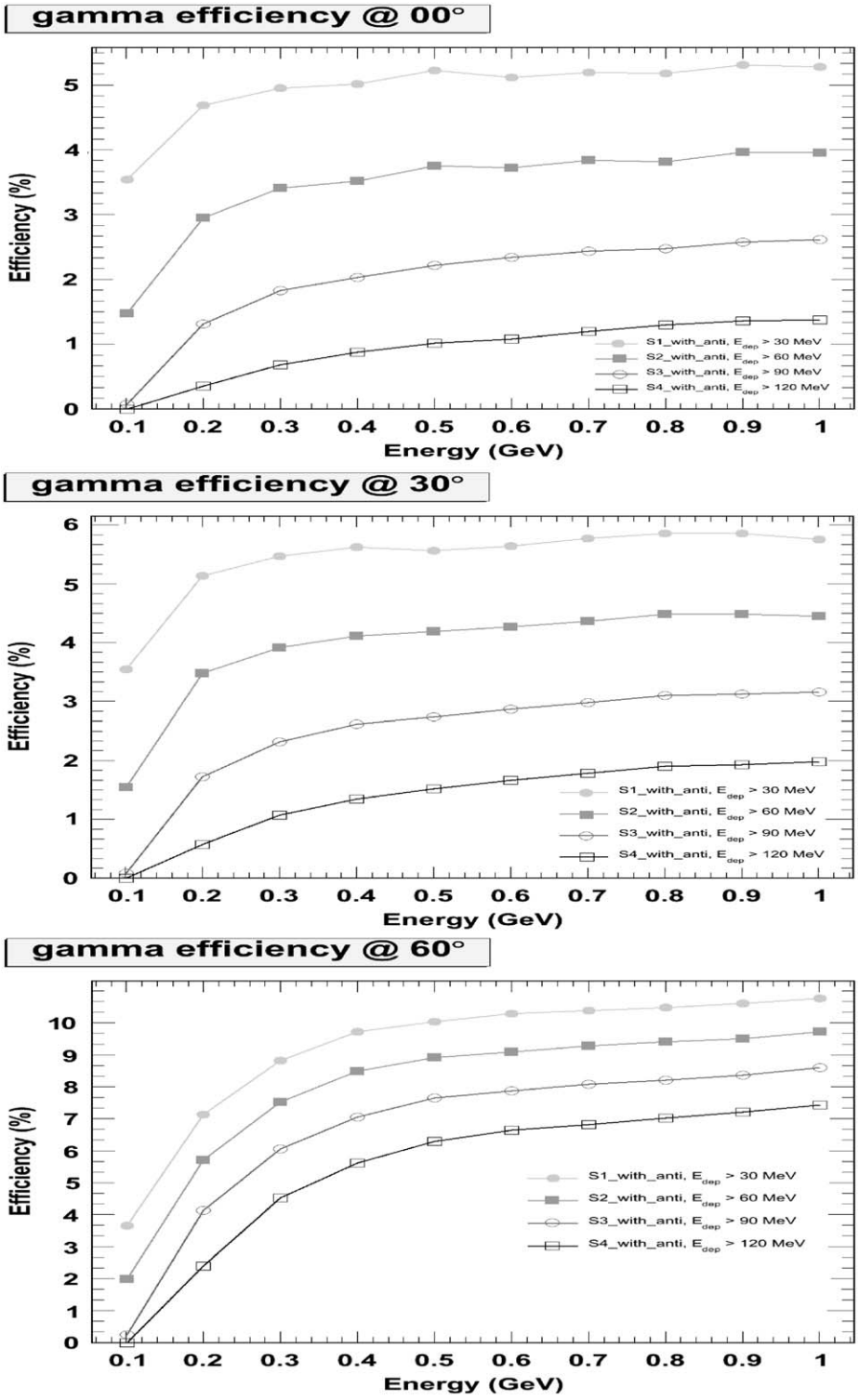

Fig. 9. Detection efficiencies of gammas for incident zenith angle at 0° (top), 30° (middle) and 60° (bottom), assuming a flux of gammas comparable to flux of neutrons.

We injected 5×10^4 particles of every species in the simulations to estimate the efficiency of the SNT and its capability to discriminate between neutrons and other kind of particles such as protons, electrons and gammas.

We demonstrated that solar neutrons of energies of the order of a few hundred MeV can be detected with efficiencies of around, and greater than 10%. On the other hand, incoming high energy protons are rejected in the neutron channels with efficiency greater than 99%. Taking into account that the fluxes of high energy electrons and gammas are much lower than those of protons and/or neutrons, the contributions of these particles to our SNT counting rates are negligible.

The angular resolutions obtained with our simulations are also in very good agreement with real data taken during the event of September 7, 2005, constituting an extra validation of the simulation code.

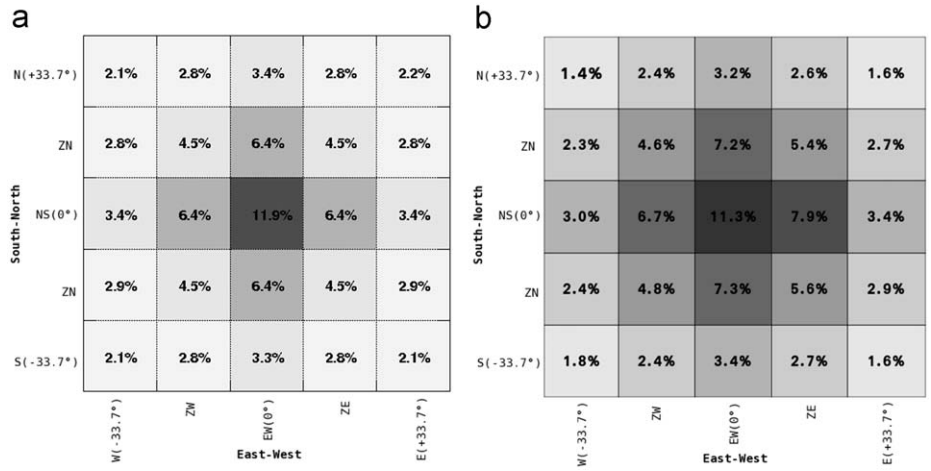

Fig. 10. (a) A simulated vertical flux of neutrons with plane energy distribution in the range of 100–1000 MeV. (b) A real SNT event registered on September 7, 2005 at 11:40 LT by SNT at Sierra Negra.

References

[1] J.F. Valdés-Galicia, et al., Nucl. Instr. and Meth. A 535 (2004).
[2] S. Agostinelli, et al., Nucl. Instr. and Meth. A 506 (2003) http://geant4.web.cern.ch/geant4.
[3] V.L. Biermann, et al., Z. Naturforsch. 6 (1951) 47.
[4] J.F. Valdés-Galicia, et al., Adv. Spac. Res. 43 (2009) 565.
[5] E.L. Chupp, et al., Astrophys. Lett. 263 (1982) L95.
[6] E.L. Chupp, et al., Astrophys. J. 318 (1987) 913.
[7] Y. Muraki, et al., Astrophys. J. 400 (1992) L75.
[8] K. Watanabe, et al., Adv. Space Res. 39 (2007) 1462.
[9] Watanabe, K. et al., Proceedings of the 30th ICRC, vol.1, 2008, p. 45.
[10] Sako, T. et al., Proceedings of the 30th ICRC, vol.1, 2008, p. 53.
[11] A. Chilingarian, et al., Nucl. Instr. and Meth. A 574 (2007).
[12] M., Moser, Ph.D. Thesis, Bern University, Switzerland, 2002.
[13] K., Watanabe, Ph.D. Thesis, Nagoya University, Japan, 2005.
[14] P. Grieder, Cosmic Rays at Earth, Researcher's Reference Data Book, Elsevier, 2001.
[15] J. Ryan, J. Geophys. Res. 82 (25) (1977) 3593.
[16] A. Bogomolov, et al., Radiat. Meas. 26 (3) (1996) 531.